



Impact of Gaussian Beam Spot Size on Trapping Forces: Continuous versus Pulsed Beams

M. A. Shukri ^{1*} and F. M. Thabit ¹

¹Physics Department , Faculty Of Science, Sana'a University, Sana'a, Yemen.

*Corresponding author: mshukri@su.edu.ye

ABSTRACT

Theoretically, this study investigates the influence of Gaussian beam spot size on the trapping forces exerted on dielectric particles by continuous and pulsed beams. We analyzed the dependence of trapping efficiency on spot size in terms of both the force value and force influence area. Our theoretical framework considers a dielectric sphere immersed in a water medium and irradiated by these beams. The results demonstrated that pulsed Gaussian beam achieves superior and more consistent trapping efficiency compared to continuous beam for a wider range of spot sizes.

ARTICLE INFO

Keywords:

Gaussian beam, Continuous Wave (CW), Pulsed beam, Rayleigh particles, Optical force, Trapping force, Beam spot size.

Article History:

Received: 31-May-2024,

Revised: 19-June-2024,

Accepted: 29-June-2024,

Available online: 30 June 2024.

1. INTRODUCTION

Optical trapping that also known as optical tweezers, utilizes tightly focused laser beams to manipulate minute particles with exceptional precision [1]. This non-invasive and contactless technique has fundamentally transformed research in medicine and biophysics. It empowers scientists to trap, sort, and study individual cells, allowing them to delve into the intricate workings of biomolecules [2–8]. Beyond its transformative impact in these fields, optical tweezers have become indispensable tools across diverse scientific disciplines, including quantum physics, optics, and chemistry [9–13]. When a tightly focused laser beam traps a particle, it exerts two main forces: the gradient force and the scattering force. The gradient force arises from the variation in the beam's intensity and pulls the particle towards the region of highest intensity. The scattering force, on the other hand, pushes the particle along the direction the light is traveling [14]. Laser beams have revolutionized various scientific fields [15–17], offering a precise tool for manipulating mesoscopic objects [18–20]. Among these, Gaussian beams (GBs) stand out for their unique intensity profile, resembling a bell curve. This characteristic allows for focused manipulation without damaging delicate samples [21–27]. However, within the realm

of Gaussian beams lie two distinct entities: continuous wave (CW) and pulsed beams. While they share the Gaussian intensity profile, their energy delivery methods set them apart, leading to unique advantages and applications. Continuous wave beams offer a constant, gentle flow of light ideal for delicate samples due to their lower peak power and minimal thermal damage [28, 29]. In contrast, pulsed beams deliver short, intense bursts with much higher peak power, making them suitable for overcoming stronger forces or inducing non-linear effects in materials [30, 31]. Both types of Gaussian beams find applications in various fields, with CW beams excelling in initial trapping, biological studies, and atom manipulation [28, 32, 33], while pulsed beams shine in manipulating smaller particles, micromachining, and remote sensing [23, 34–37]. Understanding these distinct characteristics unlocks the potential of Gaussian beams for manipulating matter at the microscopic level, driving advancements in diverse research areas. This study explores how Gaussian beam spot size affects nanoparticle trapping force, comparing continuous and pulsed beams. The insights gained from this work hold promise for significant advancements in the design of optical tweezers. The theoretical framework is presented in Section 2, followed by a discussion of the results in Section 3. Finally,

Section 4 summarizes the key conclusions drawn from this research.

2. THEORETICAL FORMULATION

We consider a dielectric sphere with radius a and refractive index n_p immersed in a water medium with refractive index n_m and irradiated by either continuous or pulsed Gaussian beams, as depicted schematically in Fig.1. One key measurable parameter for evaluating the optical

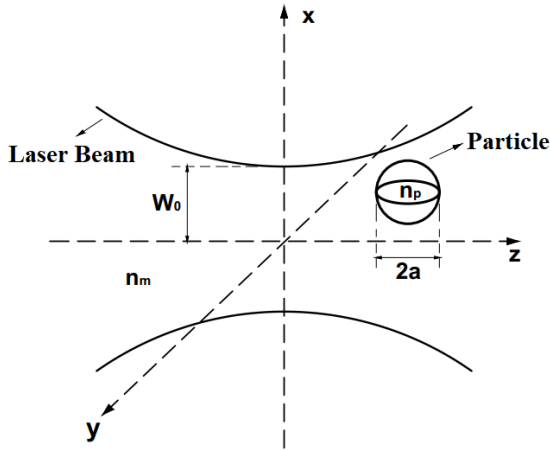


Figure 1. Schematic Diagram for laser beams radiating on a particle.

force exerted by continuous Gaussian beam is the irradiance at a specific position. This irradiance is described by the following equation [22, 38, 39]:

$$I(\tilde{\rho}, \tilde{z}) = \hat{e}_z \frac{2P}{\pi w_0^2 (1 + 4\tilde{z}^2)} \exp\left[-\frac{2\tilde{\rho}^2}{1 + 4\tilde{z}^2}\right], \quad (1)$$

where \hat{e}_z is a unit vector in the beam propagation direction, P is the input power of the beam, w_0 is the beam spot size, ρ is the transverse coordinate, z is the axial coordinate, $(\tilde{\rho}, \tilde{z}) = (\rho/w_0, z/kw_0^2)$ are dimensionless parameters, $k = \frac{2\pi}{\lambda}$ is the wave number and λ is the wave length. The dipole moment of the small sphere in the electric field located at its center is given by [22]

$$\mathbf{p}(\rho, z) = \gamma \mathbf{E}(\rho, z), \quad (2)$$

where $\gamma = 4\pi n_m^2 \epsilon_0 a^3 \left(\frac{m^2-1}{m^2+2}\right)$ is the polarizability of a spherical particle in the Rayleigh regime and $m = \frac{n_p}{n_m}$ is the relative refractive index of the particle. The optical force exerted on the particle in the Rayleigh regime can be described by two components acting on the dipole, the first is the gradient force due to the Lorentz force acting on the dipole induced by the electromagnetic field. By using the electric dipole moment of Eq.(2) as an electrostatic analogy of the electromagnetic wave, a gradient force is defined by [22]

$$\mathbf{F}_g(\mathbf{r}, t) = [\mathbf{p}(\mathbf{r}, t) \cdot \nabla] \mathbf{E}(\mathbf{r}, t) = \frac{\gamma}{2} \nabla E^2(\mathbf{r}, t). \quad (3)$$

The gradient force which the particle experiences in a steady state is the time-average version of Eq.(3) and given by

$$\mathbf{F}_g(\mathbf{r}) = \langle \mathbf{F}_g(\mathbf{r}, t) \rangle_T = \frac{\gamma}{2n_m \epsilon_0 c} \nabla I(\mathbf{r}). \quad (4)$$

A further practical expression of the gradient force in its calculation can be obtained by substituting Eq.(1) into Eq.(4) as follows:

$$\mathbf{F}_{g\rho}^{GB}(\tilde{\rho}, \tilde{z}) = -4 \hat{e}_\rho \frac{\chi \tilde{\rho}}{w_0 (1 + 4\tilde{z}^2)} I(\tilde{\rho}, \tilde{z}), \quad (5)$$

$$\begin{aligned} \mathbf{F}_{gz}^{GB}(\tilde{\rho}, \tilde{z}) &= -8 \hat{e}_z \frac{\chi \tilde{z}}{k w_0^2 (1 + 4\tilde{z}^2)} I(\tilde{\rho}, \tilde{z}) \\ &\times \left[1 - \frac{2\tilde{\rho}^2}{1 + 4\tilde{z}^2}\right], \end{aligned} \quad (6)$$

where $\chi = \frac{\gamma}{2n_m \epsilon_0 c}$. The second force component is the scattering force, which is much smaller than the gradient force for the small Rayleigh particles. This scattering force is given by [22]

$$\mathbf{F}_{Scat}^{GB}(\tilde{\rho}, \tilde{z}) = \hat{e}_z \frac{n_m}{c} C_p I(\tilde{\rho}, \tilde{z}), \quad (7)$$

where $C_p = \left(\frac{8\pi}{3}\right)(ka)^4 a^2 \left(\frac{m^2-1}{m^2+2}\right)^2$ is the cross section of the radiation pressure of the spherical particles in the Rayleigh regime. The expression for the intensity of pulsed Gaussian beam is given by [40]:

$$\begin{aligned} I(\tilde{\rho}, \tilde{z}, \tilde{t}) &= \hat{e}_z \frac{2\sqrt{2}U}{\pi^{3/2} \tau w_0^2 (1 + 4\tilde{z}^2)} \\ &\times \exp\left[-\frac{2\tilde{\rho}^2}{1 + 4\tilde{z}^2} - 2\left(\tilde{t} - \frac{\tilde{z}k w_0^2}{c\tau}\right)^2\right], \end{aligned} \quad (8)$$

where U is the input energy, τ is the pulse duration, $c = \frac{1}{\sqrt{\epsilon_0 \mu_0}}$ is the speed of light in vacuum, ϵ_0 and μ_0 are the permittivity and permeability in the vacuum respectively. The force exerted on the dielectric sphere by the light beam at position \mathbf{r} is determined by the Lorentz force, defined as a sum of electric \mathbf{E} and magnetic \mathbf{B} contributions [41]

$$\mathbf{F}(\mathbf{r}, t) = [\mathbf{p}(\mathbf{r}, t) \cdot \nabla] \mathbf{E}(\mathbf{r}, t) + \frac{\partial \mathbf{p}(\mathbf{r}, t)}{\partial t} \times \mathbf{B}(\mathbf{r}, t). \quad (9)$$

After some mathematical relations and identities in Eq.(9), we get

$$\begin{aligned} \mathbf{F}(\rho, z, t) &= \\ &\hat{e}_\rho \frac{\gamma}{2} \frac{\partial |E_x|^2}{\partial \rho} + \hat{e}_z \frac{\gamma}{2} \frac{\partial |E_x|^2}{\partial z} + \hat{e}_z \frac{\gamma n_m}{c} \frac{\partial |E_x|^2}{\partial t}, \end{aligned} \quad (10)$$

where $I(\rho, z, t) = \frac{n_m \epsilon_0 c}{2} |E_x(\rho, z, t)|^2$. The first term in Eq.(10) represents the transverse component of gradient force ($F_{g\rho}$), the second term represents the axial component of gradient force (F_{gz}) and the last term represents the F_t force which arises due to the presence of the pulse term. We can obtain all components of pulsed GB force

as follows:

$$F_{g\rho}(\tilde{\rho}, \tilde{z}, \tilde{t}) = -\hat{\mathbf{e}}_{\rho} \frac{4\gamma\tilde{\rho}I(\tilde{\rho}, \tilde{z}, \tilde{t})}{n_m\epsilon_0 c w_0 (1+4\tilde{z}^2)}, \quad (11)$$

$$F_{gz}(\tilde{\rho}, \tilde{z}, \tilde{t}) = -\hat{\mathbf{e}}_z \frac{4\gamma I(\tilde{\rho}, \tilde{z}, \tilde{t})}{n_m\epsilon_0 c} \times \left[\frac{\tilde{z}k w_0^2}{\tau^2 c^2} - \frac{\tilde{t}}{\tau c} + \frac{1}{2\tilde{z}k w_0^2} \left(1 - \frac{1}{1+4\tilde{z}^2}\right) \left(1 - \frac{2\tilde{\rho}^2}{1+4\tilde{z}^2}\right) \right], \quad (12)$$

$$F_t(\tilde{\rho}, \tilde{z}, \tilde{t}) = -\hat{\mathbf{e}}_z \frac{8\gamma\mu_0\tilde{t}}{\tau} I(\tilde{\rho}, \tilde{z}, \tilde{t}) + \hat{\mathbf{e}}_z \frac{8\gamma\mu_0\tilde{z}k w_0^2}{\tau^2 c} I(\tilde{\rho}, \tilde{z}, \tilde{t}). \quad (13)$$

These equations (11-13) are equivalent to the equations (9-11) found in reference [40]. The scattering force F_{Scat} caused by the scattering of light by the sphere is proportional with light intensity and along the direction of light propagation. The scattering force can be expressed as[40]:

$$F_{Scat}(\tilde{\rho}, \tilde{z}, \tilde{t}) = \hat{\mathbf{e}}_z \frac{n_m}{c} C_p I(\tilde{\rho}, \tilde{z}, \tilde{t}). \quad (14)$$

3. RESULTS AND DISCUSSION

On the light of theoretical foundation established earlier in section 2, this section presents a series of key results alongside their detailed discussions. The figures throughout this section were generated using the following parameters, unless otherwise specified: $\lambda = 0.5145 \mu m$, $U = 0.1 \mu J$, $P = 100 mW$, $n_p = 1.59$ (Silica) and $n_m = 1.332$ (water). For clarity in interpreting figures 2 and 5, a color coding is employed to indicate the direction of the optical force. Yellow-red region represents a force directed upwards and to the right, whereas yellow-blue region represents a force directed downwards and to the left. Figure 2 illustrates the relationship between the transverse ($F_{g\rho}$) and axial (F_{gz}) gradient forces of a continuous Gaussian beam as well as the total axial force ($F_z = F_{gz} + F_{scat}$) exerted on a nano-dielectric particle in both the transverse (ρ) and axial (z) directions for different values of beam spot size (w_0). Our results demonstrate a significant decrease in the optical forces ($F_{g\rho}$, F_{gz} , and F_z) as the beam spot size increases. This decrease is attributed to the distribution of the beam intensity over a larger spot size. Interestingly, the area affected by the gradient forces appears to remain independent of the beam spot size as shown in sub-figures 2(a-h). The results also reveal stable trapping region along both the transverse at ($\rho = 0$) and axial at ($z = 0$) directions due to the transverse and axial gradient forces, respectively. This indicates that the particle experiences a net force towards the center of the beam in these regions. However, the forces guiding the particle also play a role. The transverse gradient force guides the particle along the axial direction at $z = 0$ and $\rho = \pm 0.5 w_0$ as

shown in sub-figures 2(a-d). Similarly, the axial gradient force guides the particle along the transverse direction at $\rho = 0$ and $z = \pm 0.5 k w_0^2$ as shown in sub-figures 2(e-h). Including the effect of the scattering force, as shown in sub-figures 2(i-l), reveals a stable trapping region for beam spot size (w_0) less than $3 \mu m$. However, for beam spot size greater than or equal to $3 \mu m$, the scattering force becomes dominant compared to the axial gradient force. This dominance of the scattering force disrupts the trapping mechanism, leading to the absence of stable trapping in this case. Figure 3 illustrates the

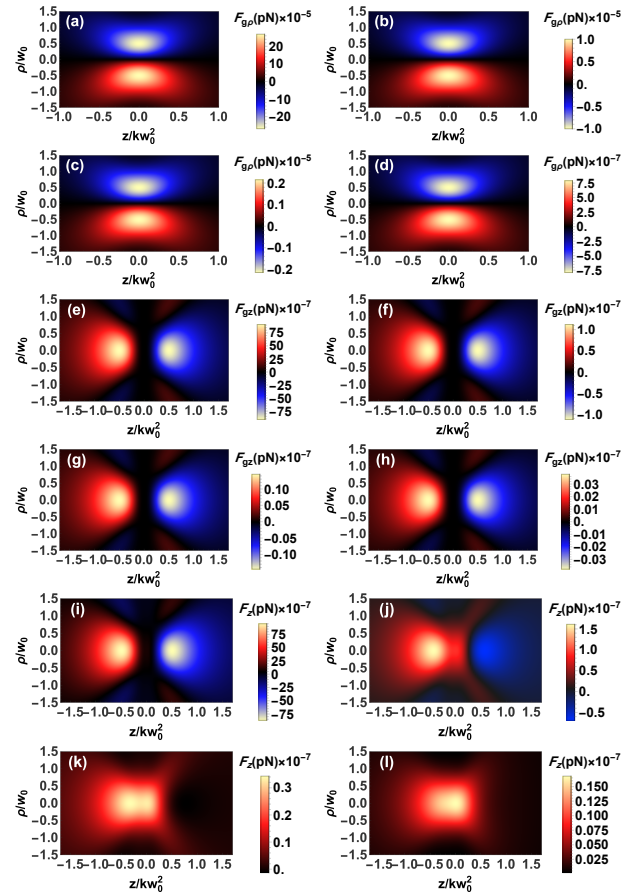


Figure 2. Shows the behavior of the optical forces of continuous Gaussian beam along the transverse and axial directions at $a = 10 nm$. (a-d) For the transverse gradient force $F_{g\rho}$, (e-h) for the axial gradient force F_{gz} and (i-l) for the total axial force F_z . (a,e,i) $w_0 = 1 \mu m$, (b,f,j) $w_0 = 3 \mu m$, (c,g,k) $w_0 = 5 \mu m$, (d,h,l) $w_0 = 7 \mu m$.

influence of beam spot size (w_0) on the relationship between the scattering force (F_{scat}) and the axial direction (z) of continuous GB. This figure demonstrates a significant decrease in scattering force (F_{scat}) as the beam spot size (w_0) increases. Also, the area affected by this force remains independent of w_0 . Furthermore, comparing the axial gradient force (sub-figures 2(e-h)) with the scattering force (Fig. 3) for corresponding beam spot sizes reveals a critical point: when w_0 reaches or exceeds $3 \mu m$, the scattering force becomes comparable to the axial

gradient force. This competition between forces disrupts the trapping mechanism, leading to the absence of stable trapping at larger beam spot sizes. Figure 4 depicts the

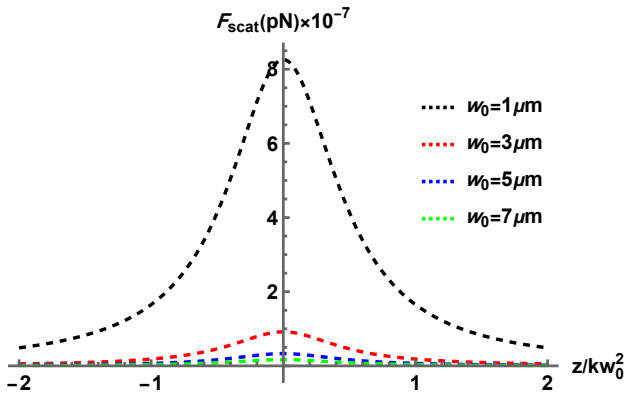


Figure 3. Shows the relationship between the scattering force (F_{scat}) and the axial direction (z) of continuous GB at $a = 10\text{ nm}$ and for different values of beam spot size (w_0).

dependence of the maximum forces ($F_{g\rho}$ and F_z) on the beam spot size (w_0) for a continuous Gaussian beam. The results clearly demonstrate a decrease in both the maximum transverse gradient force ($F_{g\rho}$) and the maximum total axial force (F_z) with increasing beam spot size. This decrease is likely attributed to the distribution of the beam intensity over a larger area as w_0 increases. Interestingly, the maximum values of $F_{g\rho}$ consistently exceed those of F_z . This suggests that the trapping efficiency in the transverse direction is stronger compared to the axial direction. Figure 5 explores the dependence of the optical forces ($F_{g\rho}$, $F_{gz}+F_t$ and F_z) on beam spot size (w_0) for a pulsed Gaussian beam with a pulse duration of $\tau = 0.1\text{ ps}$ and a particle radius of $a = 10\text{ nm}$. Sub-figures 5(a-d) depict the transverse gradient force ($F_{g\rho}$) across the transverse (ρ) and axial (z) directions for various beam spot sizes. The results consistently reveal a decrease in force magnitude with increasing w_0 . Additionally, the force influence area appears to shrink as w_0 increases along the axial direction. Notably, stable trapping persists along the transverse direction at $\rho = 0$ and $z = 0$, while the guiding forces dominate along the axial direction at $z = 0$. Sub-figures 5(e-h) illustrate the behavior of the axial force ($F_{gz}+F_t$) for different beam spot sizes. Similar to the transverse case, the force weakens as w_0 increases, and the force influence area shrinks with increasing beam spot size along the axial direction. Interestingly, sub-figure (e) shows stable trapping along the axial direction at $z = 0$ and $\rho = \pm 0.3 w_0$, but only for beam spot sizes up to $w_0 \leq 2\text{ }\mu\text{m}$. Beyond this threshold ($w_0 > 2\text{ }\mu\text{m}$), sub-figures (f-h) indicate a complete absence of trapping. In this case, only the guiding force prevails across both axial and transverse directions, with its dominant locations being $\rho = 0$ and larger beam spot sizes. Sub-figures 5(i-l) depict the total axial force ($F_z =$

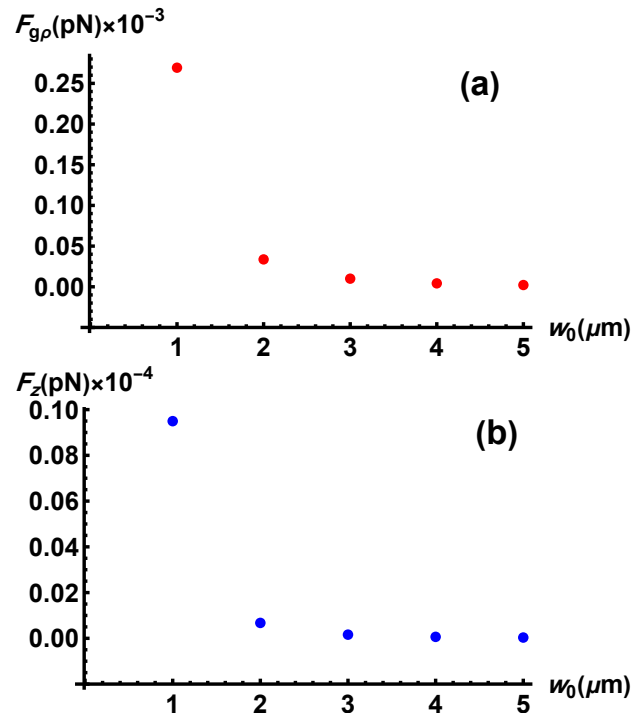


Figure 4. Presents the dependence of the maximum optical forces on the beam width (w_0) for a continuous Gaussian beam with a particle radius of $a = 10\text{ nm}$. (a) Shows the maximum transverse gradient force ($F_{g\rho}$), while (b) shows the maximum total axial force (F_z).

$F_{gz}+F_t+F_{scat}$). The force behavior mirrors the trends observed for $F_{g\rho}$ and $F_{gz}+F_t$. Stable trapping is present for $w_0 \leq 2\text{ }\mu\text{m}$ at $z = 0$ and $\rho = \pm 0.3 w_0$ (sub-figure (i)), but absent for larger beam spot sizes ($w_0 > 2\text{ }\mu\text{m}$) as shown in sub-figures (j-l). In these cases, only the guiding force prevails. In general, and by comparing the sub-figures 5(e-h) with 5(i-l), we find that the effect of beam spot size on the type of force exerted on the particle, whether it is attraction or repulsion, is greater than the effect of the scattering force. In addition, we find from sub-figures 5f and 5j that the force influence area increases significantly at a beam spot size of $3\text{ }\mu\text{m}$, as it is considered the turning point of the force from attraction to repulsion. Moreover, a stronger transverse gradient force compared to the axial force significantly enhances trapping stability. Figure 6 explores the impact of beam spot size (w_0) on the scattering force (F_{scat}) acting on a pulsed Gaussian beam with a pulse duration of $\tau = 0.1\text{ ps}$ and a particle radius of $a = 10\text{ nm}$. The force is exerted along the axial direction (z) for various beam spot sizes. The results clearly reveal a significant decrease in F_{scat} with increasing w_0 . The area affected by this force decreases with increasing beam spot size. Furthermore, comparing the axial force $F_{gz}+F_t$ from sub-figures 5(e-h) with the scattering force (F_{scat}) in Fig. 6 for corresponding beam spot size (w_0) demonstrates that $F_{gz}+F_t$ is generally greater than F_{scat} . This implies a stronger trapping effect due to the combined forces

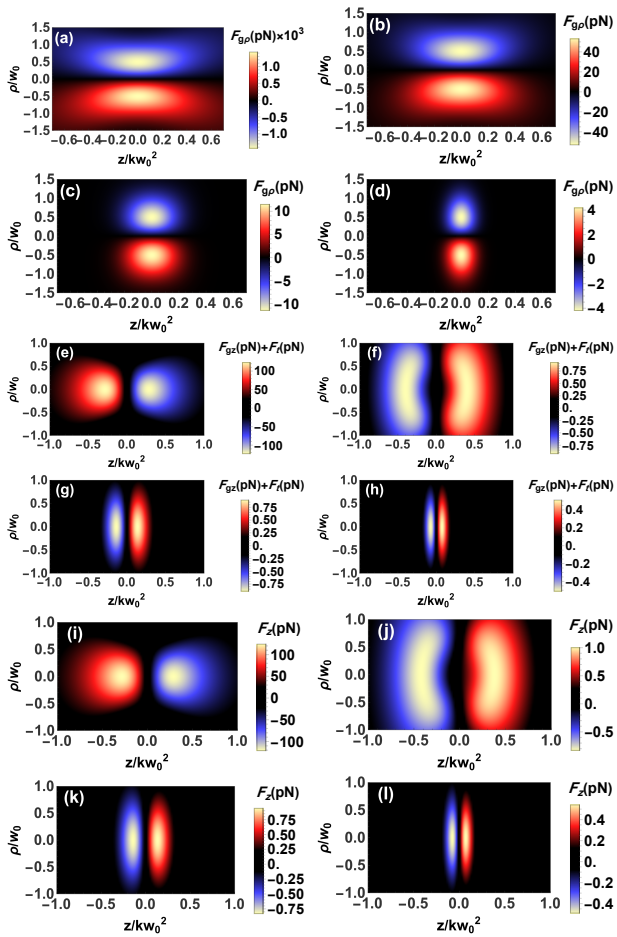


Figure 5. Shows the behavior of the optical forces of pulsed Gaussian beam along the transverse and axial directions at $a = 10 \text{ nm}$ and $\tau = 0.1 \text{ ps}$. (a-d) For the transverse gradient force $F_{g\rho}$, (e-h) for the axial force $F_{gz}+F_t$ and (i-l) for the total axial force F_z . (a,e,i) $w_0 = 1\mu\text{m}$, (b,f,j) $w_0 = 3\mu\text{m}$, (c,g,k) $w_0 = 5\mu\text{m}$, (d,h,l) $w_0 = 7\mu\text{m}$.

compared to the scattering force alone. Figure 7 depicts

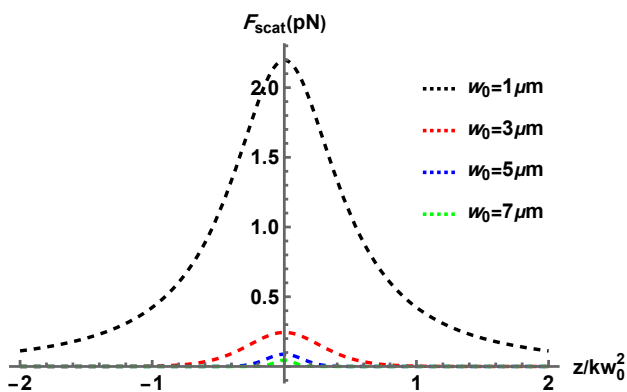


Figure 6. Shows the relationship between the scattering force (F_{scat}) and the axial direction (z) of pulsed GB for different values of beam spot size (w_0).

the dependence of the maximum forces ($F_{g\rho}$ and F_z) on the beam spot size (w_0) for a pulsed Gaussian beam. The results clearly demonstrate a decrease in both the

maximum transverse gradient force ($F_{g\rho}$) and the maximum total axial force (F_z) with increasing beam spot size. This decrease is likely attributed to the distribution of the beam intensity over a larger area as w_0 increases. Interestingly, the maximum values of $F_{g\rho}$ consistently exceed those of F_z . This suggests that the trapping efficiency in the transverse direction is stronger compared to the axial direction.

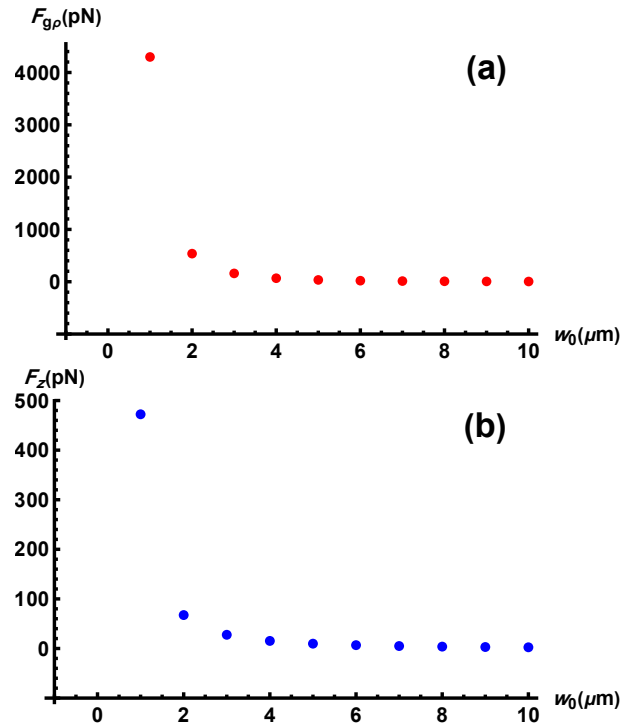


Figure 7. Presents the dependence of the maximum optical forces on the beam spot size (w_0) for a pulsed Gaussian beam with a pulse duration $\tau = 0.1 \text{ ps}$ and a particle radius of $a = 10 \text{ nm}$. (a) Shows the maximum transverse gradient force ($F_{g\rho}$), while (b) shows the maximum total axial force (F_z).

4. CONCLUSIONS

By comparing the pulsed and continuous Gaussian beams and analyzing their results, we conclude the following: The force exerted by the pulsed beam is significantly greater than that of the continuous beam. Axial trapping in the continuous beam is more susceptible to the scattering force and wider beam spot size. In contrast, axial trapping in the pulsed beam is more affected by an increase in beam spot size, causing the force to transition from attraction to repulsion at larger beam spot sizes. Transverse trapping, regardless of whether it occurs in a continuous or pulsed beam, exhibits greater stability for any suitable beam spot size due to its force values being significantly larger than those of the axial force. The area of force influence is dependent on the beam spot size in the pulsed beam and remains unaffected in the continuous beam. This characteristic could be advantageous for increasing the number of particles trapped or guided within the same area. Based on the

mentioned points, the pulsed beam is considered

REFERENCES

- [1] M. J. Padgett, J. Molloy, and D. McGloin, *Optical Tweezers: Methods and Applications* (CRC Press, 2010).
- [2] K. Dholakia, M. P. MacDonald, P. Zemánek, and T. Imr, "Cellular and colloidal separation using optical forces," *Methods Cell Biol.* **82**, 467–495 (2007).
- [3] T. A. Nieminen, G. Knoner, N. R. Heckenberg, and H. Rubinsztein-Dunlop, "Physics of optical tweezers," in *Methods in Cell Biology*, vol. 82 (2007), pp. 207–236.
- [4] H. Xin, Y. Li, Y.-C. Liu, *et al.*, "Optical forces: From fundamental to biological applications," *Adv. Mater.* **32**, 2001994 (2020).
- [5] C. A. Campugan, K. R. Dunning, and K. Dholakia, "Optical manipulation: A step change for biomedical science," *Contemp. Phys.* **61**, 277–294 (2020).
- [6] H. L. *et al.*, "Optical pulling forces and their applications," *Adv. Opt. Photonics* **12**, 288–366 (2020).
- [7] K. Dholakia, B. W. Drinkwater, and M. Ritsch-Marte, "Comparing acoustic and optical forces for biomedical research," *Nat. Rev. Phys.* **2**, 480–491 (2020).
- [8] I. A. Favre-Bulle and E. K. Scott, "Optical tweezers across scales in cell biology," *Trends Cell Biol.* **32**, 932–946 (2022).
- [9] M. J. Lang and S. M. Block, "Resource letter: Lbot-1: Laser-based optical tweezers," *Am. J. Phys.* **71**, 201 (2003).
- [10] C.-Y. Chuang, M. Zammit, M. L. Whitmore, and M. J. Comstock, "Combined high-resolution optical tweezers and multi-color single-molecule fluorescence with an automated single-molecule assembly line," *The J. Phys. Chem. A* **123**, 9612–9620 (2019).
- [11] J. M. *et al.*, "Optomechanics with levitated particles," *Rep. Prog. Phys.* **83**, 026401 (2020).
- [12] E. Otte and C. Denz, "Optical trapping gets structure: Structured light for advanced optical manipulation," *Appl. Phys. Rev.* **7**, 041308 (2020).
- [13] H. Hwang, A. Byun, J. Park, *et al.*, "Optical tweezers throw and catch single atoms," *Optica* **10**, 401–406 (2023).
- [14] G. Pesce, P. H. Jones, O. M. Maragò, and G. Volpe, "Optical tweezers: Theory and practice," *Eur. Phys. J. Plus* **135**, 1–38 (2020).
- [15] S. Kumar and M. J. Deen, *Fiber optic communications: fundamentals and applications* (John Wiley & Sons, 2014).
- [16] F. Thabit, A. Alkelly, and M. Shukri, "Propagation of fully and partially coherent flat-topped multi-gaussian beams through axicons," *JOSA A* **37**, 759–767 (2020).
- [17] H. Wang, D. Deng, Z. Zhai, and Y. Yao, "Laser-processed functional surface structures for multi-functional applications—a review," *J. Manuf. Process.* **116**, 247–283 (2024).
- [18] A. Ashkin and J. M. Dziedzic, "Optical trapping and manipulation of viruses and bacteria," *Science* **235**, 1517–1520 (1987).
- [19] D. G. Grier, "A revolution in optical manipulation," *Nature* **424**, 810–816 (2003).
- [20] D. S. Bradshaw and D. L. Andrews, "Manipulating particles with light: radiation and gradient forces," *Eur. J. Phys.* **38**, 034008 (2017).
- [21] A. Ashkin, J. M. Dziedzic, J. E. Bjorkholm, and S. Chu, "Observation of a single-beam gradient force optical trap for dielectric particles," *Opt. Letters* **11**, 288–290 (1986).
- [22] Y. Harada and T. Asakura, "Radiation forces on a dielectric sphere in the rayleigh scattering regime," *Opt. Commun.* **124**, 529–541 (1996).
- [23] L.-G. Wang and C.-L. Zhao, "Dynamic radiation force of a pulsed gaussian beam acting on a rayleigh dielectric sphere," *Opt. Express* **15**, 10615–10621 (2007).
- [24] J. Li, S. Zhuang, and C. Huang, "Gradient force evolution of gaussian beam induced by a phase plate," *Opt. Lasers Engineering* **46**, 595–600 (2008).
- [25] D. J. Stevenson, F. Gunn-Moore, and K. Dholakia, "Light forces the pace: optical manipulation for biophotonics," *J. Biomedical Optics* **15**, 041503–041503 (2010).
- [26] L.-G. Wang and H.-S. Chai, "Revisit on dynamic radiation forces induced by pulsed gaussian beams," *Opt. Express* **19**, 14389–14402 (2011).
- [27] M.-C. Zhong, Z.-Q. Wang, and Y.-M. Li, "Oscillations of absorbing particles at the water-air interface induced by laser tweezers," *Opt. Express* **25**, 2481–2488 (2017).
- [28] A. Ashkin, "Optical trapping and manipulation of neutral particles using lasers," *Opt. Lett.* **24**, 54–56 (1999).
- [29] L. Novotny and B. Hecht, *Principles of Nano-Optics* (Cambridge University Press, 2012).
- [30] Y. Jiang, T. Narushima, and H. Okamoto, "Nonlinear optical effects in trapping nanoparticles with femtosecond pulses," *Nat. Phys.* **6**, 1005–1009 (2010).
- [31] L. Gong, B. Gu, G. Rui, *et al.*, "Optical forces of focused femtosecond laser pulses on nonlinear optical rayleigh particles," *Photonics Res.* **6**, 138–143 (2018).
- [32] A. Ashkin, "History of optical trapping and manipulation of small neutral particles, atoms, and molecules," *Single Mol. Spectrosc.* pp. 1–31 (2001).
- [33] Z. Gong, Y.-L. Pan, G. Videen, and C. Wang, "Optical trapping and manipulation of single particles in air: Principles, technical details, and applications," *J. Quant. Spectrosc. Radiat. Transf.* **214**, 94–119 (2018).
- [34] J. C. Shane, M. Mazilu, W. M. Lee, and K. Dholakia, "Effect of pulse temporal shape on optical trapping and impulse transfer using ultrashort pulsed lasers," *Opt. Express* **18**, 7554–7568 (2010).
- [35] L. Cerami, E. Mazur, S. Nolte, and C. B. Schaffer, "Femtosecond laser micromachining," in *Ultrafast Nonlinear Optics*, (2013), p. 287–321.
- [36] N. du Preez-Wilkinson, A. B. Stilgoe, T. Alzaidi, *et al.*, "Forces due to pulsed beams in optical tweezers: Linear effects," *Opt. Express* **23**, 7190–7208 (2015).
- [37] T.-H. Liu, W.-Y. Chiang, A. Usman, and H. Masuhara, "Optical trapping dynamics of a single polystyrene sphere: Continuous wave versus femtosecond lasers," *The J. Phys. Chem. C* **120**, 2392–2399 (2016).
- [38] F. Thabit and M. Shukri, "Trapping of low and high refractive index nano-spherical particles by using a highly focused laguerre–gaussian beam," *Appl. Opt.* **63**, 2614–2620 (2024).
- [39] M. Shukri and F. Thabit, "Calculation of trapping optical forces induced by a focused continuous hermite gaussian beam on a nano-dielectric spherical particle," *Phys. Scripta* **99**, 065504 (2024).
- [40] M. Shukri and F. Thabit, "Calculation of the optical forces exerted on a nano-dielectric sphere induced by a pulsed laguerre–gaussian beam," *JOSA A* **40**, 645–651 (2023).
- [41] J. P. Gordon, "Radiation forces and momenta in dielectric media," *Phys. Rev. A* **8**, 14 (1973).